

Note: This is a preprint of a paper submitted for publication. Contents of this paper should not be quoted or referred to without permission of the author(s).

CONF-951007--24

Presented at 188th Meeting of the Electrochemical Society, Chicago, Illinois, October 8-13, 1995 and published in *Thin-Film Solid Ionic Devices and Materials*, ed. by J. B. Bates, Electrochemical Society, Pennington, New Jersey.

SPUTTER DEPOSITION AND CHARACTERIZATION OF LITHIUM
COBALT OXIDE THIN FILMS AND THEIR APPLICATIONS IN
THIN-FILM RECHARGEABLE LITHIUM BATTERIES

B. Wang, J. B. Bates, C. F. Luck, B. C. Sales, and R. A. Zuhr
Solid State Division, Oak Ridge National Laboratory
Oak Ridge, TN 37831-6030

and

J. D. Robertson
Department of Chemistry, University of Kentucky, Lexington, KY 40502

"The submitted manuscript has been authored by a contractor of the U.S. Government under contract No. DE-AC05-96OR22464. Accordingly, the U.S. Government retains a nonexclusive, royalty-free license to publish or reproduce the published form of this contribution, or allow others to do so, for U.S. Government purposes."

Prepared by
SOLID STATE DIVISION
OAK RIDGE NATIONAL LABORATORY
Managed by
LOCKHEED MARTIN ENERGY RESEARCH CORP.
under
Contract No. DE-AC05-96OR22464
with the
U.S. DEPARTMENT OF ENERGY
Oak Ridge, Tennessee

January 1996

MASTER

DISTRIBUTION OF THIS DOCUMENT IS UNLIMITED

pic

SPUTTER DEPOSITION AND CHARACTERIZATION OF LITHIUM COBALT OXIDE THIN FILMS AND THEIR APPLICATIONS IN THIN-FILM RECHARGEABLE LITHIUM BATTERIES

B. Wang, J. B. Bates, C. F. Luck, B. C. Sales, and R. A. Zuhr
Solid State Division, Oak Ridge National Laboratory, Oak Ridge, TN 37831-6030
and
J. D. Robertson
Department of Chemistry, University of Kentucky, Lexington, KY 40502

ABSTRACT

Lithium cobalt oxide thin films have been deposited by rf magnetron sputtering of a LiCoO_2 target in a 3:1 Ar/O₂ mixture gas. From proton-induced γ -ray emission analysis (PIGE) and Rutherford backscattering spectrometry (RBS), the average composition of these films was determined to be $\text{Li}_{1.15}\text{CoO}_{2.16}$. The x-ray powder diffraction patterns of films annealed in air at 500–700°C were consistent with the regular rhombohedral structure observed for crystalline LiCoO_2 . The discharge curves of thin film lithium cells with amorphous LiCoO_2 showed no obvious structural transition between 4.2 V and 1.5 V. The shape of the discharge curves of the cells with polycrystalline cathodes were consistent with a two-phase voltage plateau at ~3.9 V with a relatively large capacity and two additional smaller plateaus at higher voltages. Cells with the 700°C annealed cathodes showed a capacity loss of ~1% after 1000 cycles between 4.2 V and 3.0 V.

INTRODUCTION

Lithium cobalt oxide has been investigated as a cathode material in rechargeable lithium batteries (1–5). The structure of LiCoO_2 consists of alternate layers of lithium and cobalt atoms that occupy the octahedral sites of a rhombohedral lattice (6). Lithium ions can be reversibly extracted from the layers with a corresponding change of cobalt oxidation. Recently, thin films of lithium cobalt oxide have been used as the counter electrode in electrochromic windows and as the cathode in lithium ion batteries (7–10).

Thin-film lithium batteries based on V_2O_5 and LiMn_2O_4 cathodes have been investigated in this laboratory for several years (11–13). To extend our study to other cathode materials, we have investigated the properties of LiCoO_2 films deposited by magnetron sputtering and their behavior in thin-film rechargeable lithium cells.

FILM GROWTH AND CHARACTERIZATION

Lithium cobalt oxide films were deposited by planar rf magnetron sputtering of single LiCoO_2 targets onto 2000 Å thick Pt current collectors on the Coors' ADS-996 alumina plates. In several cases, films were simultaneously deposited onto graphite

substrates for ion beam and nuclear reaction analysis. The target was prepared by cold pressing and sintering powders of pure LiCoO_2 (Alfa, 99.5%) at 900°C for 2 hours. After processing, the target measured 2" in diameter by about 3 mm thick. The flow of Ar and O_2 into the vacuum chamber was regulated at about 12–5 sccm total flow to maintain a 3/1 Ar/ O_2 ratio and a constant pressure of 20 mTorr. Assuming a film density of 5.06 g/cm^3 , the deposition rate measured before and after deposition with a quartz crystal thickness monitor positioned 5 cm above the target was typically 7–12 Å/min at a net applied rf power of 40–50 W. After sputtering the target for 1h, the substrates were rotated into position 5 cm above the target. The emission spectrum of the plasma was recorded periodically using the setup described previously (14). The nearly constant intensity of a lithium emission line at $\sim 671 \text{ nm}$ to that of an argon line at $\sim 750 \text{ nm}$ together with a deposition rate that was approximately the same before and after deposition indicated of a steady sputtering process. The cathode films were deposited through an aluminum mask that defined a $11 \text{ mm} \times 11 \text{ mm}$ area. The cathodes ranged in thickness from 0.3–0.5 μm as measured with a profilometer, in good agreement with the estimated thickness from the rate measurements assuming a theoretical density of 5.06 g/cm^3 . Based on this density, the estimated mass of the cathodes was 0.2–0.3 mg. After deposition, some cathodes were annealed at $500\text{--}700^\circ\text{C}$ for two hours in air and slowly cooled to room temperature.

The compositions of the cathode films deposited onto graphite substrates were determined using proton-induced γ -ray emission analysis (PIGE) to obtain Li/Co ratios and Rutherford backscattering spectrometry (RBS) to obtain the Co/O ratios. An example of an RBS spectrum is shown in Fig. 1; the solid line is the simulated backscattering from which the Co/O ratios were obtained. The Li/Co and O/Co ratios determined by PIGE and RBS were $1.15 (\pm 0.02)$ and $2.16 (\pm 0.13)$, respectively, giving an average film composition of $\text{Li}_{1.15}\text{CoO}_{2.16}$.

Powder X-ray diffraction measurements of the thin films were made with a Scintag diffractometer using $\text{Cu } K\alpha$ radiation and a high-purity Ge detector. Data were collected in the 2θ range of $10\text{--}70^\circ$ at a scan rate of $3^\circ/\text{min}$. The as-deposited films were X-ray amorphous. An example of a diffraction pattern of an annealed LiCoO_2 film on a Coors' alumina substrate is shown in Fig. 2. After annealing, a peak appeared at $2\theta = 18.64$ which can be assigned to diffraction from the (003) planes of the $\alpha\text{-NaFeO}$ structure of LiCoO_2 .

The dc resistivity of one of the annealed films was measured as a function of temperature using a four probe method and silver paint contacts. The results are shown in Fig. 3. The resistivity of the film increased with decreasing temperature, characteristic of a semiconductor, and the room temperature resistivity was $\sim 2 \Omega\cdot\text{cm}$. Previous thermoelectric studies on bulk and thin films indicate that LiCoO_2 is a p -type semiconductor and that electron holes are the majority carriers (7).

CELL MEASUREMENTS

After the characterizing the LiCoO_2 films, thin film cells were constructed following the procedures described elsewhere (11–13). The cathodes were covered with about $1 \mu\text{m}$ of amorphous lithium phosphorus oxynitride (Lipon) electrolyte deposited by rf magnetron sputtering of Li_3PO_4 in N_2 . This material has a typical composition of $\text{Li}_{2.9}\text{PO}_{3.3}\text{N}_{0.46}$ and a conductivity of $2 \times 10^{-6} \text{ S}\cdot\text{cm}^{-1}$ at 25°C (15). Lithium anode films about $3 \mu\text{m}$ thick were

then deposited over the electrolyte by evaporation of lithium metal contained in a Ta crucible at a pressure of about 10^{-6} Torr. The cells were tested either in an argon-filled glove box or in vacuum tight stainless steel bottles using 1 mA channels of a Maccor battery test system. The cells were cycled at constant current between specified voltage limits. At the end of the charge cycles, the voltage was held constant until the current decreased to about $1 \mu\text{A}$.

Examples of the initial charge curve and discharge curves at different current densities of cells with an as-deposited X-ray amorphous and high-temperature annealed polycrystalline cathodes are shown in Fig. 4a-d. For the as-deposited cathode, the discharge curves have a characteristic s-shape with no evidence of a phase change, similar to the behavior observed in thin-film lithium cells with amorphous V_2O_5 cathodes (11). For the cells with the annealed cathodes, a knee in the charge-discharge curves at about 3.9 V marks the onset of a first order phase transition from LiCoO_2 to Li_xCoO_2 ($x < 1$) in which the lattice expands along the *c*-axis (1-3) as lithium is extracted from the cathode. The flat voltage plateau at ~ 3.93 V and the associated sharp peak in the plot of $-\text{dq}/\text{dV}$ vs. V shown in Fig. 5 is characteristic of a two phase region. The co-existence of two phases in this region was confirmed by Reimers and Dahn (3) who reported the appearance of two Bragg peaks in the in-situ diffraction pattern of bulk LiCoO_2 when the cell voltage was about 3.93 V. From the value of *x* in Li_xCoO_2 given in Fig. 4d, which was based on the estimated cathode mass and the assumption that $x = 1$ at the onset of the charge curve, the two phase region is seen to extend from $x = 1$ to $x \sim 0.75$.

At values of $x < 0.65$, two additional plateaus at higher voltages, seen as small inflections in the discharge curve of Fig. 4, give rise to peaks in the $-\text{dq}/\text{dV}$ vs. V plot at about 4.07 and 4.17 V (Fig. 5). Reimers and Dahn (3) have attributed these features to an order-disorder phase transition involving rearrangement of the lithium ions and a change in the lattice from hexagonal to monoclinic symmetry occurring at $x \sim 0.5$. No additional features were observed on charging the cells to 4.6 V or on discharging them to 1.5 V.

The decrease in voltage with increasing discharge current evident in the curves in Fig. 4 is due to the internal resistance of the cells. The resistances of the cells estimated by dividing the change in voltage near the midpoint of the discharge curves by the change in current density are listed in Table 1. As it can be seen, the cell resistance decreases significantly on annealing the cathode at 500°C , and continues to decrease as the annealing temperature is increased to 600°C . The internal resistivity of cell with the 700°C annealed polycrystalline LiCoO_2 cathode, $6 \times 10^6 \Omega\text{-cm}$, is comparable to that of the best polycrystalline LiMn_2O_4 thin-film cell studied in this laboratory, $2 \times 10^6 \Omega\text{-cm}$ (13). We have found from the analysis of ac impedance measurements that in all cases the cell resistance is determined by the mobility of Li^+ ions in the cathode (12). The lithium diffusion in the layered polycrystalline LiCoO_2 thin-film cathode is fast and results in the low internal cell resistance. When the layered structure is disordered as in the as-deposited amorphous cathode, lithium diffusion is slow and leads to a high internal cell resistance.

The results of cycling two cells with cathodes annealed at 500°C and 700°C between 4.2 V and 3.0 V at a current density of $100 \mu\text{A}/\text{cm}$ are shown in Fig. 6. As illustrated in Fig. 4d, the major capacity loss occurs on the first discharge following the initial charge of a new cell. The initial loss, in this case about 5%, is true loss of active cathode material, evidently due to a reduction in available lithium sites since less lithium is inserted than removed. Thereafter, the capacity loss is caused primarily by an increase in the resistance of the cathode and the cathode-electrolyte interface as a result of a decrease in lithium ion

mobility. For the cell with the cathode annealed at 500°C, the rate of capacity fading was higher on the first 200 cycles but then decreased gradually with continued cycling. The increase in cell resistance which caused the capacity loss was perhaps due to a change in the structure of the cathode with insertion and removal of Li⁺. By contrast, the cell with the more highly crystallized, 700°C annealed cathode exhibited a much smaller capacity loss that remained constant at about 0.001%/cycle throughout cycling.

Table I. Resistance of Li-LiCoO₂ Thin Film Batteries as Estimated from the Discharge Curves at Different Current Densities.

Cathode	Thickness (μm)	Cell Resistance (Ω)
As deposited	0.30	8058
500°C annealed	0.47	1267
600°C annealed	0.46	331
700°C annealed	0.48	452

CONCLUSIONS

Thin films of lithium cobalt oxide deposited by rf magnetron sputtering of LiCoO₂ in Ar + O₂ have compositions close to that of the target material. Annealing of the as-deposited X-ray amorphous films in air at temperatures from 500–700°C results in the formation of polycrystalline material with the same rhombohedral structure and electrochemical properties observed for bulk LiCoO₂ synthesized at high temperatures. Thin film lithium cells with 700°C annealed LiCoO₂ cathodes have low internal resistances and small capacity losses with cycling.

ACKNOWLEDGMENTS

This research was supported by The Department of Energy's Division of Materials Sciences, Division of Chemical Science, Office of Energy Research Technology Transfer Program, and Office of Transportation Technologies under contract No. DE-AC05-96OR22464 with Lockheed Martin Energy Research Corp. The DOE sponsored appointment of BW to the Oak Ridge National Laboratory Postdoctoral Research Program which is administered by the Oak Ridge Institute for Science and Education.

REFERENCES

1. K. Mizushima, P. C. Jones, P. J. Wiseman and J. B. Goodenough, *Mat. Res. Bull.*, **15**, 783 (1980).

2. E. Plichta, S. Slane, M. Uchiyama and M. Salomon, *J. Electrochem. Soc.* **136**, 1865 (1989).
3. J. N. Reimers and J. Dahn, *J. Electrochem. Soc.*, **139**, 2091 (1992).
4. R. J. Gummow, M. M. Thackeray, W. I. F. David and S. Hull, *Mat. Res. Bull.*, **27**, 327 (1992).
5. K. Ozawa, *Solid State Ionics*, **69**, 212 (1994).
6. H. J. Orman and P. J. Wiseman, *Acta Cryst.*, **C40**, 12 (1984).
7. G. Wei, T. E. Hass and R. B. Goldner, *Solid State Ionics*, **58**, 115 (1992).
8. R. B. Goldner, S. Slaven, T. Y. Liu, T. E. Haas, F. Q. Arntz and P. Zerigian, *Mat. Res. Soc. Symp. Proc.*, G-A. Nazri, J-M. Tarascon and M. Schreiber, Editors, **369**, p. 137, MRS, Pittsburgh, PA (1995).
9. C. H. Chen, A. A. J. Buysman, E. M. Kelder and J. Schoonman, *Solid State Ionics*, **80**, 1 (1995).
10. M. Antaya, J. R. Dahn, J. S. Preston, E. Rossen and J. N. Reimers, *J. Electrochem. Soc.* **140**, 575 (1993).
11. J. B. Bates, N. J. Dudney, G. R. Gruzalski, R. A. Zuhr, A. Choudhury and C. F. Luck, *J. Power Sources*, **43-44**, 103 (1993).
12. J. B. Bates, G. R. Gruzalski, N. J. Dudney, C. F. Luck and X. Yu, *Solid State Ionics*, **70-71**, 619 (1994).
13. J. B. Bates, N. J. Dudney, D. C. Lubben, G. R. Gruzalski, B. S. Kwak, X. Yu and R. A. Zuhr, *J. Power Sources*, **54**, 58 (1995).
14. J. B. Bates, N. J. Dudney, C. F. Luck, B. C. Sales, R. A. Zuhr, and J. D. Robertson, *J. Am. Ceram. Soc.*, **76**, 929 (1993).
15. J. B. Bates, N. J. Dudney, G. R. Gruzalski, R. A. Zuhr, A. Choudhury and C. F. Luck, *Solid State Ionics*, **53-56**, 647 (1992).

DISCLAIMER

This report was prepared as an account of work sponsored by an agency of the United States Government. Neither the United States Government nor any agency thereof, nor any of their employees, makes any warranty, express or implied, or assumes any legal liability or responsibility for the accuracy, completeness, or usefulness of any information, apparatus, product, or process disclosed, or represents that its use would not infringe privately owned rights. Reference herein to any specific commercial product, process, or service by trade name, trademark, manufacturer, or otherwise does not necessarily constitute or imply its endorsement, recommendation, or favoring by the United States Government or any agency thereof. The views and opinions of authors expressed herein do not necessarily state or reflect those of the United States Government or any agency thereof.

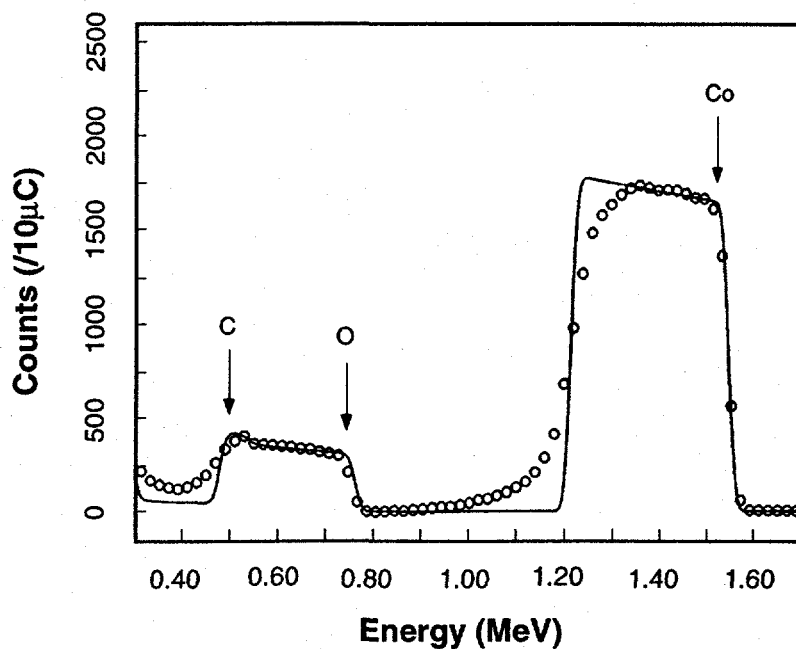


Fig. 1 RBS spectrum for LiCoO_2 thin film. Continuous line is the calculated backscattering.

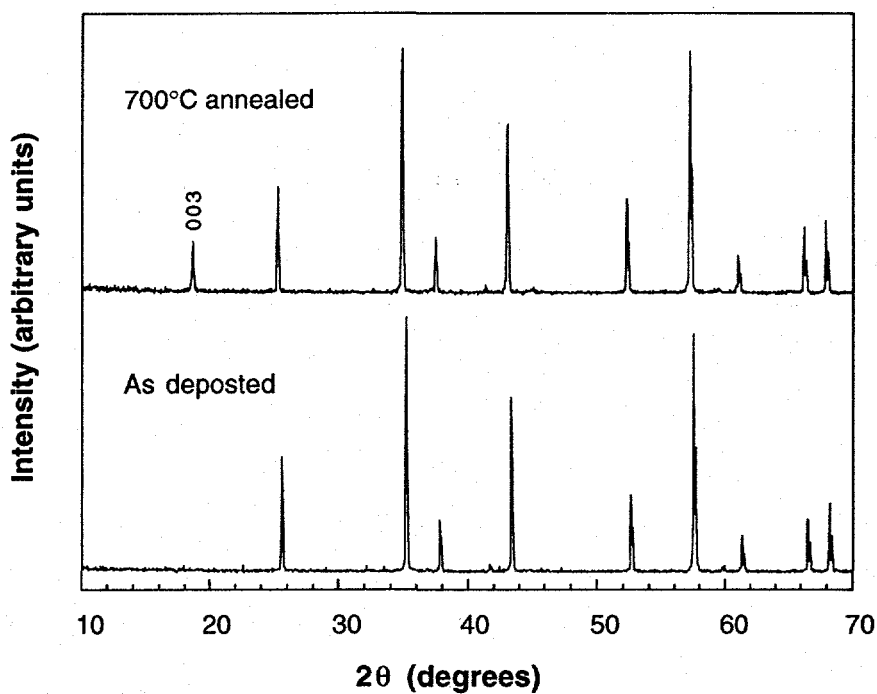


Fig. 2 X-ray powder patterns for the as-deposited and the high-temperature annealed LiCoO_2 thin films. The indexed peak is the diffraction peak from the hexagonal LiCoO_2 structure.

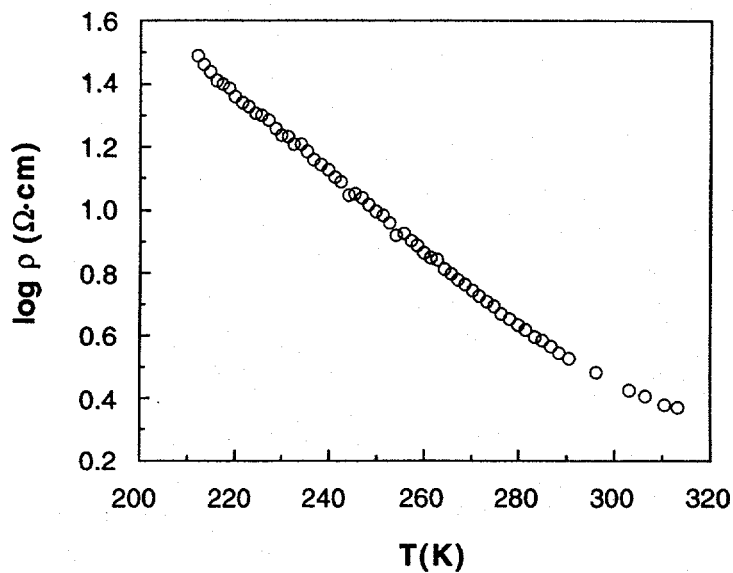


Fig. 3 Temperature dependence of the dc resistivity of a polycrystalline LiCoO_2 thin film.

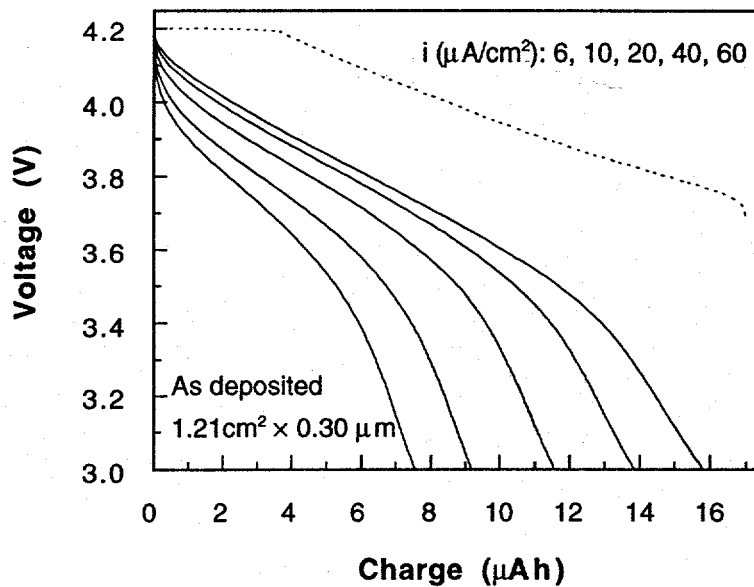


Fig. 4a Discharge curves at different current densities for a lithium cell (103E) based on an as-deposited, x-ray amorphous LiCoO_2 cathode. Dashed line is the initial charge at $50 \mu\text{A}/\text{cm}^2$

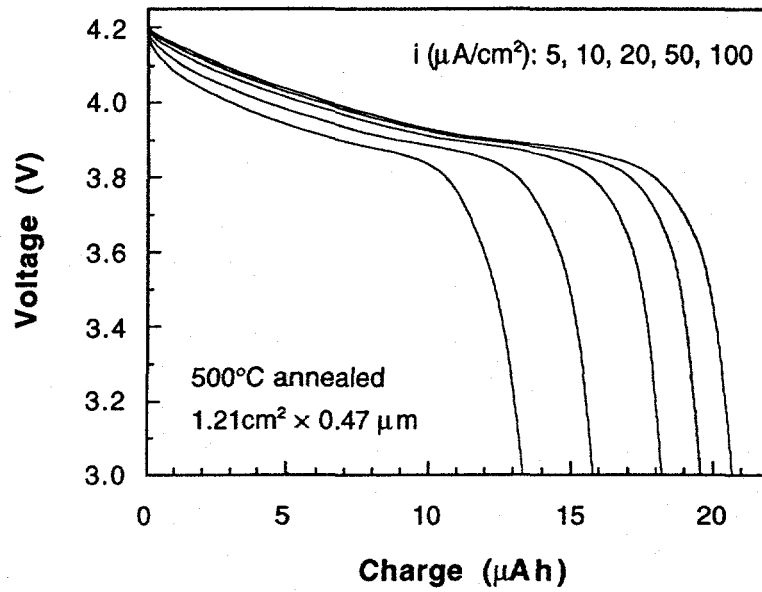


Fig. 4b Discharge curves at different current densities for a lithium cell (151EB) based on a 500°C annealed polycrystalline LiCoO_2 cathode.

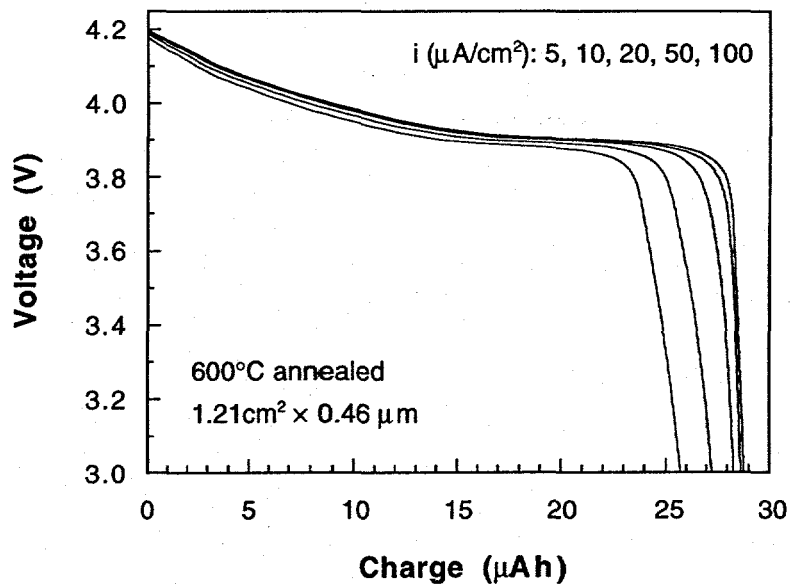


Fig. 4c Discharge curves at different current densities for a lithium cell (152EB) based on a 600°C annealed polycrystalline LiCoO_2 cathode.

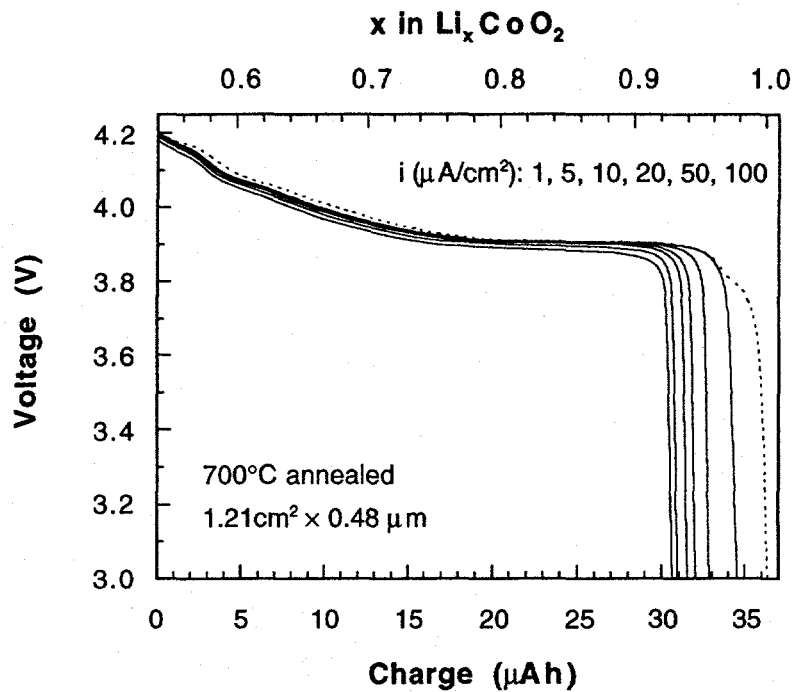


Fig. 4d Discharge curves at different current densities for a lithium cell (153EB) based on a 700°C annealed polycrystalline LiCoO_2 cathode. Dashed line is the initial charge at $1 \mu\text{A}/\text{cm}^2$.

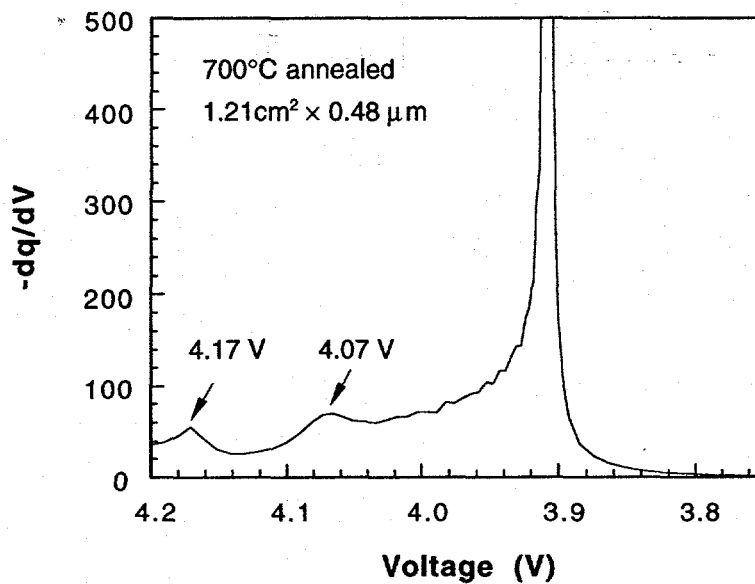


Fig. 5 The derivative $-dq/dV$ as a function of cell voltage for the lithium cell of Fig. 4d ($5 \mu\text{A}/\text{cm}^2$ discharge)

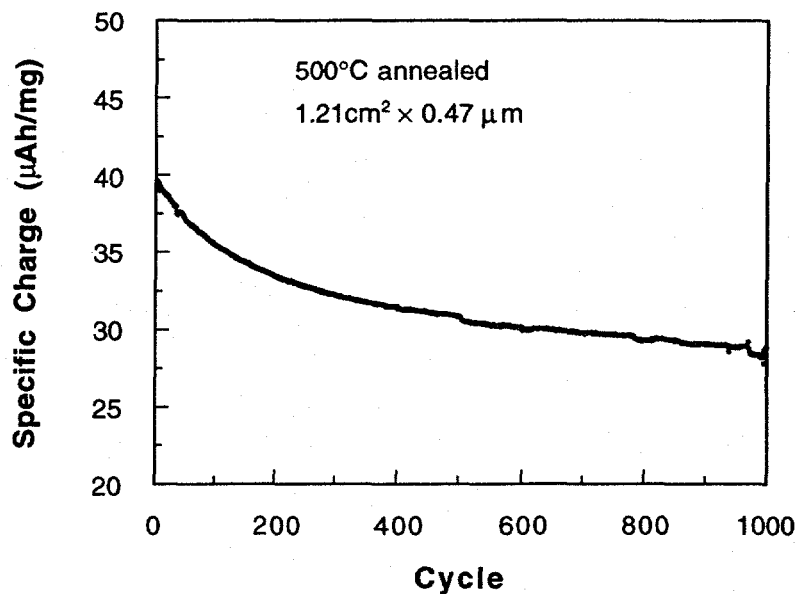


Fig. 6a Discharge capacity upon cycling between 4.2 - 3.0 V for a lithium cell (151EB) based on the 500°C annealed polycrystalline LiCoO₂ cathode at a current density of 100 μA/cm².

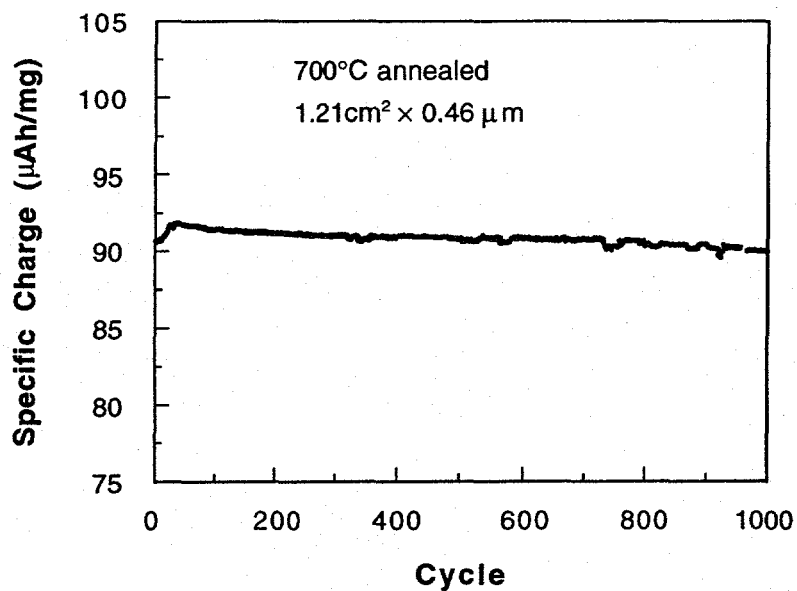


Fig. 6b Discharge capacity upon cycling between 4.2 - 3.0 V for a lithium cell (152EA) based on the 700°C annealed polycrystalline LiCoO₂ cathode at a current density of 100 μA/cm². Capacity loss ~0.001%/cycle (cycle charge ~85% of maximum capacity).